Inhibitors of the M2 proton channel engage and disrupt transmembrane networks of hydrogen-bonded waters

Jessica L. Thomaston, Nicholas F. Polizzi, Athina Konstantinidi, Jun Wang, Antonios Kolocouris, William F. DeGrado

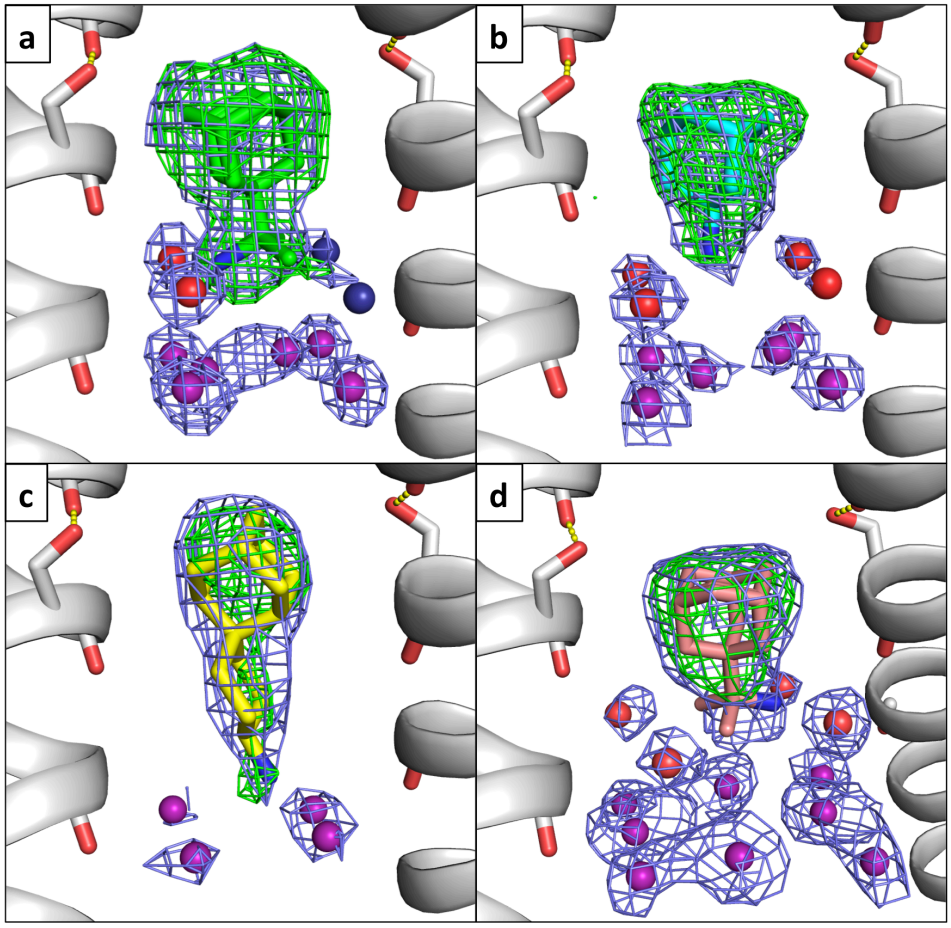

Figure S1: Electron density in channel pore above the gating His37 residues: blue mesh is 2Fo-Fc density shown at a contour of 1 σ, green mesh is a polder omit map[1] shown to a contour of 3 σ. Ala30 water layer is shown as red spheres, Gly34 water layer is shown as purple spheres. Partial occupancy waters are shown as dark blue spheres. The hydrogen bond between Ser31 and the Val27 carbonyl is shown. a. Rimantadine-bound $Inward_{closed}$ state (green, 6BKL, monomers F and H). b. Amantadine-bound $Inward_{closed}$ state (cyan, 6BKK, monomers B and D). c. Spiro-adamantyl amine-bound $Inward_{closed}$ state (yellow, 6BMZ, monomers B and D). d. Rimantadine-bound $Inward_{open}$ state (pink, 6BOC, monomers B and D). Note that, in the rimantadine-bound structures (a,d), the bound rimantadine has been modeled as a superposition of the R and S enantiomers with both at half occupancy. In the rimantadine-bound $Inward_{closed}$ structure, two of the waters in the Ala30 layer have been also been modeled as half-occupancy due to steric clashes with the rimantadine methyl group. Also note the difference in the shape of 2Fo-Fc electron

density corresponding to bridging waters in the Gly34 layer in the amantadine- and rimantadine- bound Inward$_{closed}$ state structures (a, b); these waters are two clearly defined spheres when amantadine binds to one of the tetramers (monomers A,B,C,D), though this density consists of just one water in the second tetramer within the asymmetric unit (monomers E,F,G,H); the bridging water density is elongated when rimantadine binds. This is likely caused by a racemic mixture of rimantadine enantiomers resulting in two water structures that are averaged in the electron density.

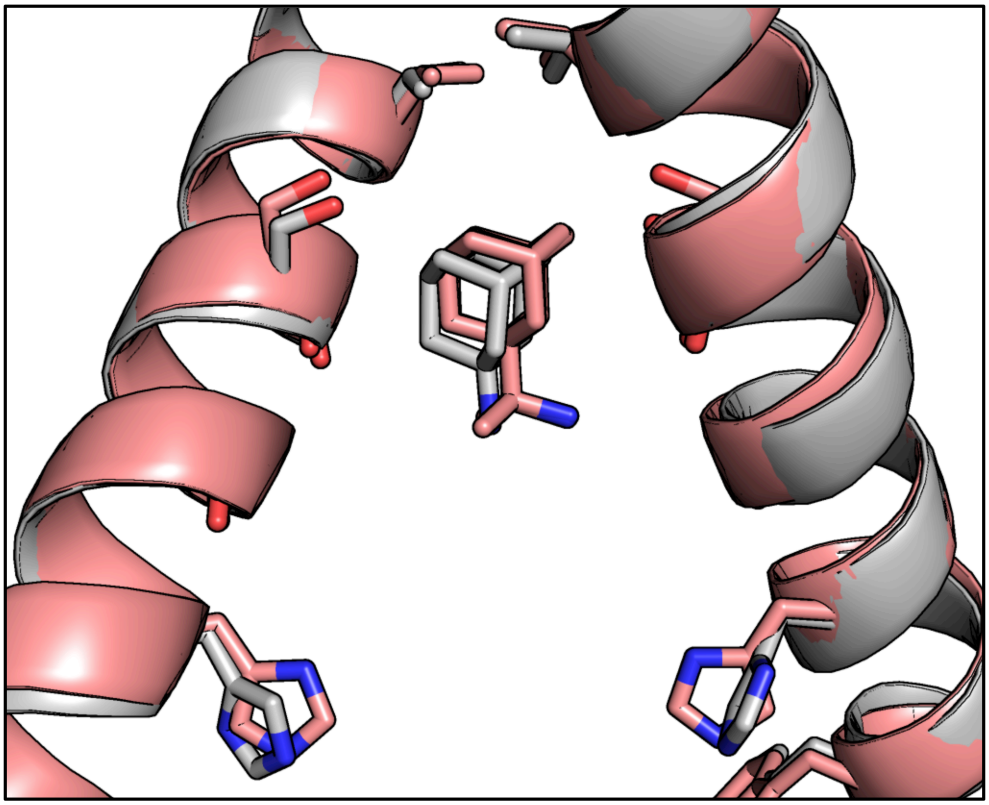

Figure S2: Aligned rimantadine-bound Inward$_{open}$ (6BOC, pink) and amantadine-bound Inward$_{open}$ (3C9J, gray) structures. The position of the bound rimantadine group is in good agreement with the previously observed binding position of amantadine. Note that the His37 rotamers in structure 3C9J are not meaningfully different, as these side chains were fit to 3.5 Å resolution electron density.

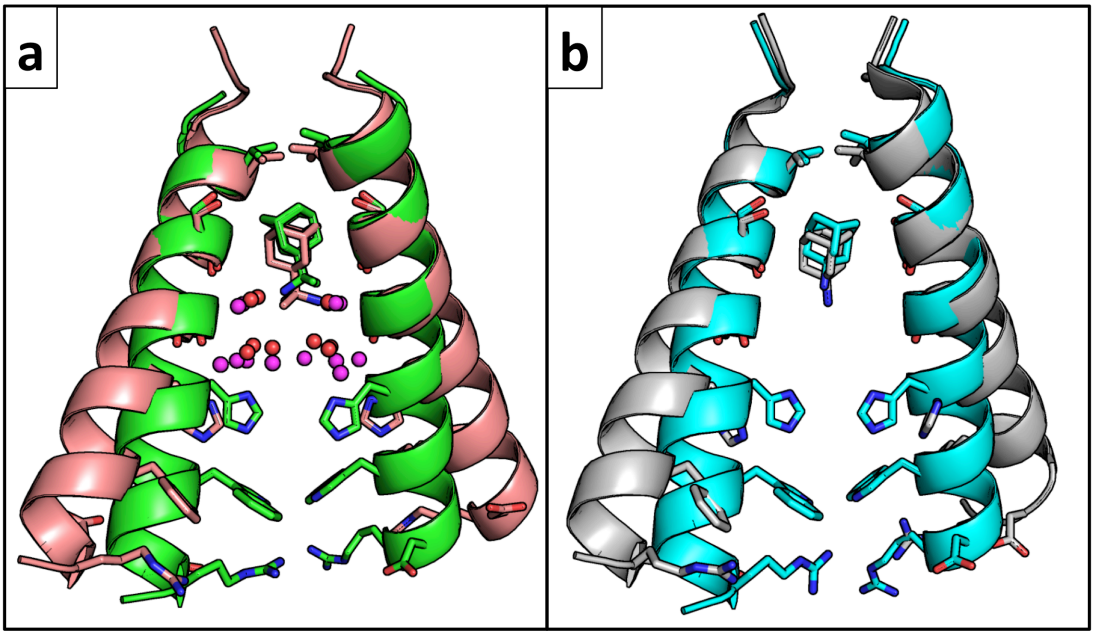

Figure S3: Alignment of Inward$_{open}$ and Inward$_{closed}$ structures showing rimantadine and amantadine binding. A: Rimantadine-bound Inward$_{open}$ (6BOC, pink with waters shown as magenta spheres) and Inward$_{closed}$ (6BKL, green with waters shown as red spheres) structures. B. Previously solved amantadine-bound Inward$_{open}$ structure (3C9J, gray)[2] and the amantadine-bound Inward$_{closed}$ structure (6BKK, cyan). In the Inward$_{open}$ conformation, the top of the pore near Val27 is constricted adamantane drugs bind slightly deeper in the channel pore.

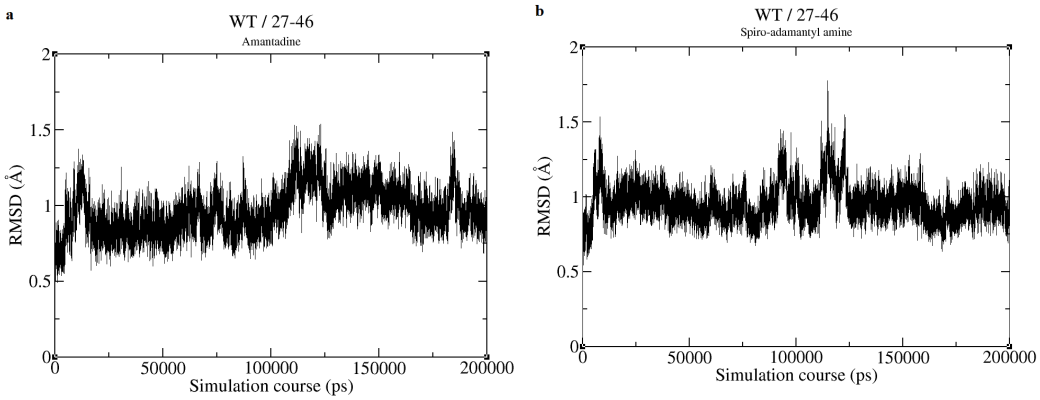

Figure S4. Cα atom RMSD during MD simulations. Root-mean-square deviation (RMSD) for Cα atoms of M2TM relative to the initial structure for MD simulations of amantadine and spiro-adamantyl amine complexes (PDB IDs: 6BKK and 6BMZ respectively), after root-mean-square fitting of Cα atoms of M2TM; values in Å. The tetramer observed in the X-ray crystal structure was maintained for all 200 ns of simulation time

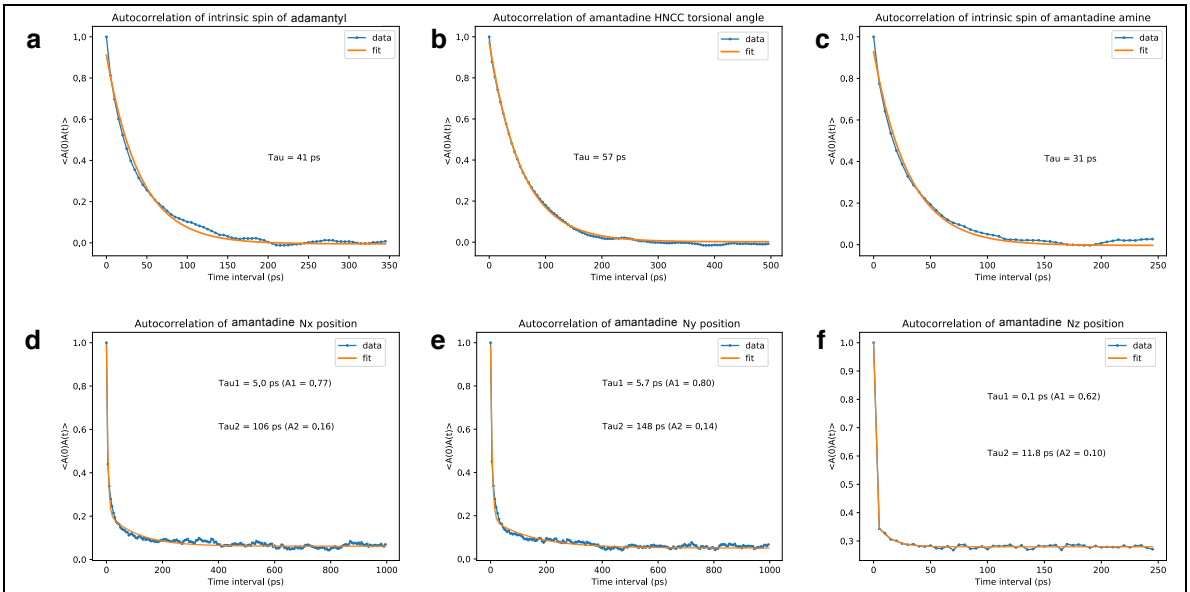

Figure S5: Autocorrelation of amantadine rotation and displacement. Correlation decay times are labeled in the insets, with corresponding amplitudes for bi-exponential fits.

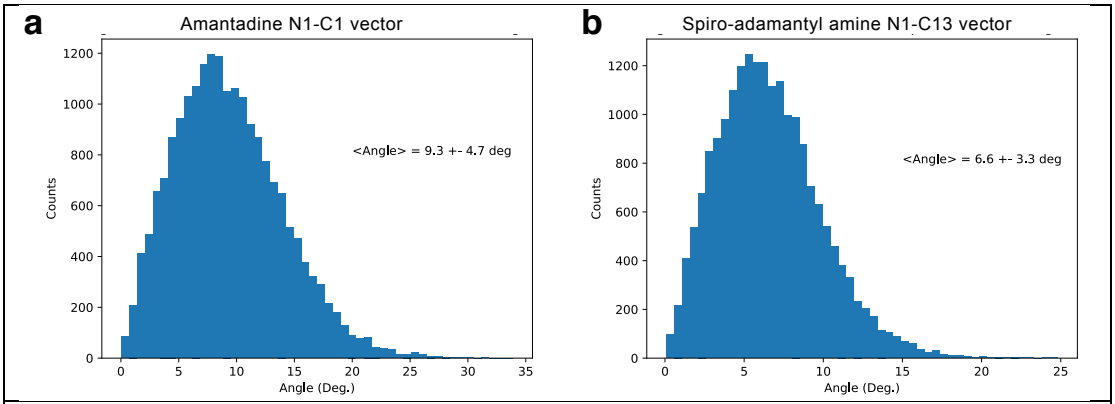

Figure S6: Histograms from 20,000 MD snapshots (5ps intervals) of tilt angle relative to bundle long axis.

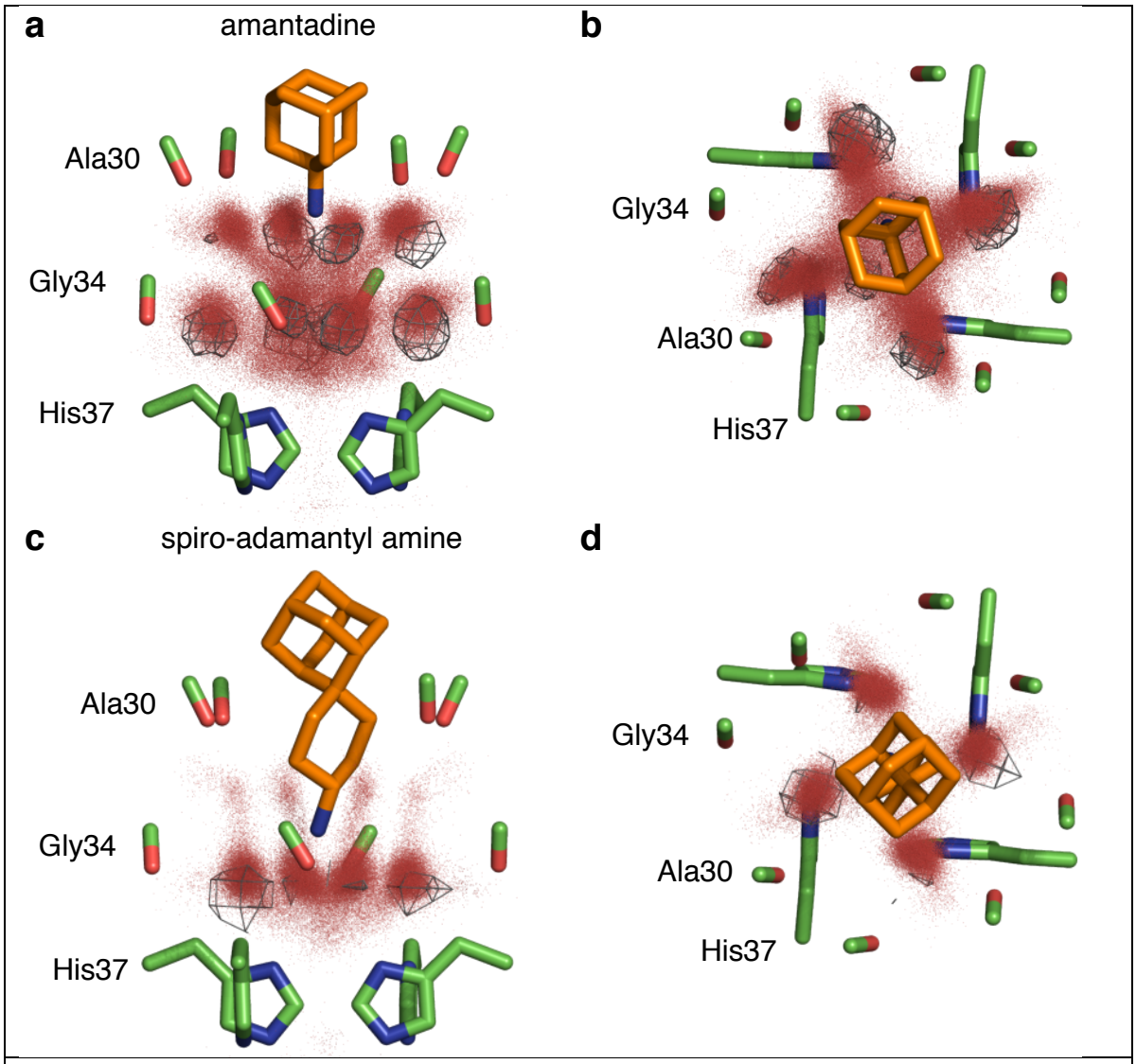

Figure S7: Molecular dynamics reproduces the positions of the crystallographic waters, all snapshots. The X-ray crystal structure is shown as sticks. Red dots are water oxygen positions from 20,000 molecular dynamics snapshots. Gray wireframe shows 1σ contours of water electron density from the X-ray crystal structure. a,c: Side views. b,d: Top views.

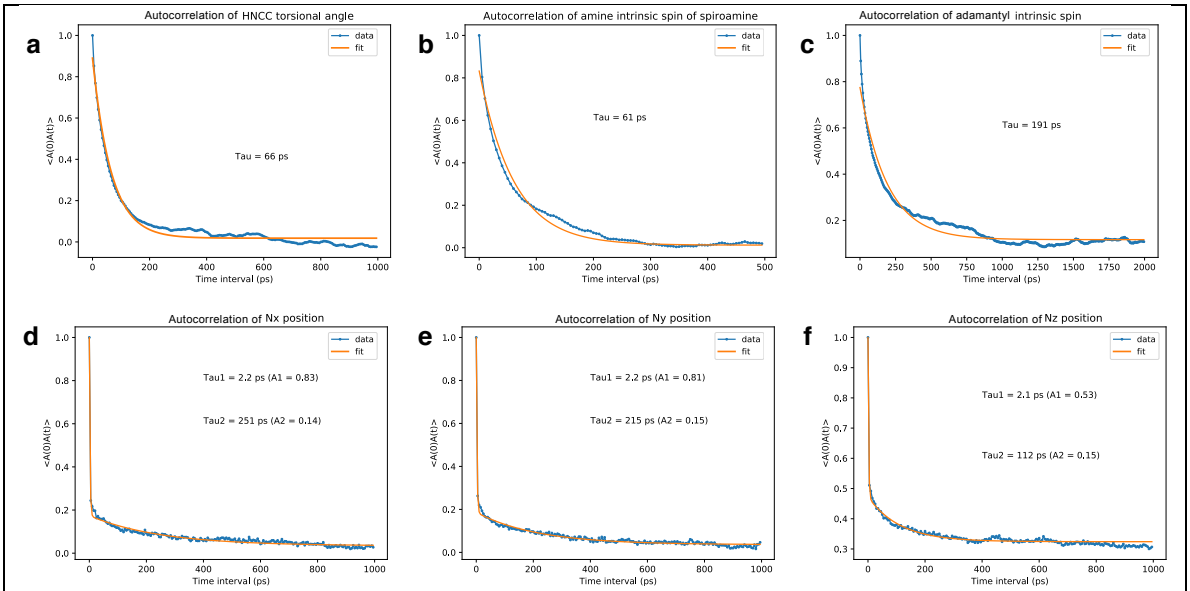

Figure S8: Autocorrelation of spiro-adamantyl amine rotation and displacement. Correlation decay times are labeled in the insets, with corresponding amplitudes for bi-exponential fits.

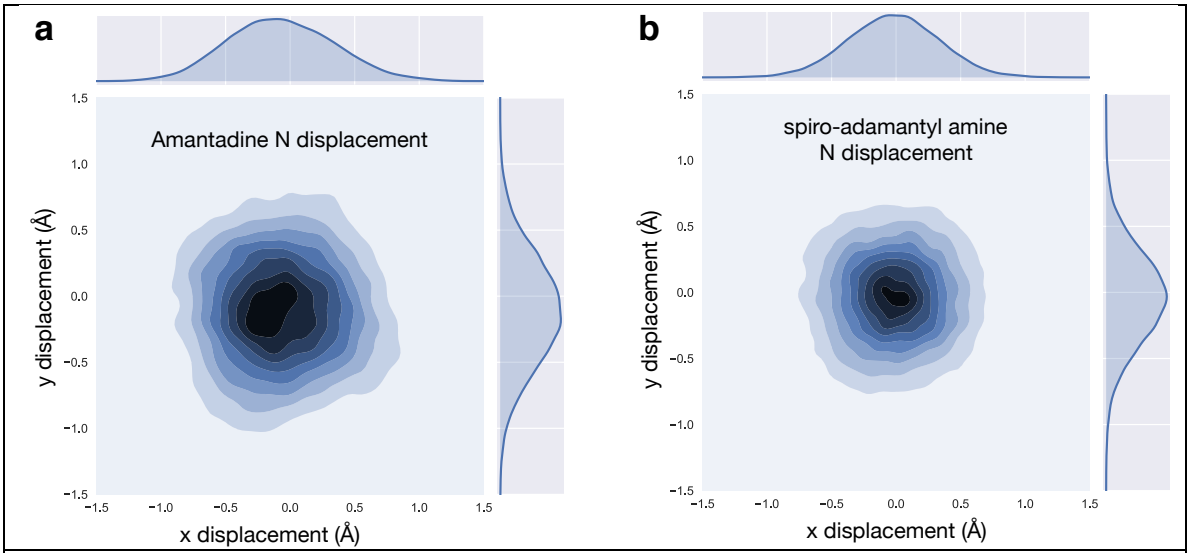

Figure S9: Kernel density estimate (KDE) of the amine N displacement of amantadine (a) and spiro-adamantyl amine (b) in the x-y plane (orthogonal to bundle long-axis). Darker shading represents higher density, e.g., near (-0.3, -0.3) in (a) showing the amine N spends a substantial amount of time off-center. KDEs are derived from 20,000 snapshots (5 ps intervals) of the MD simulation.

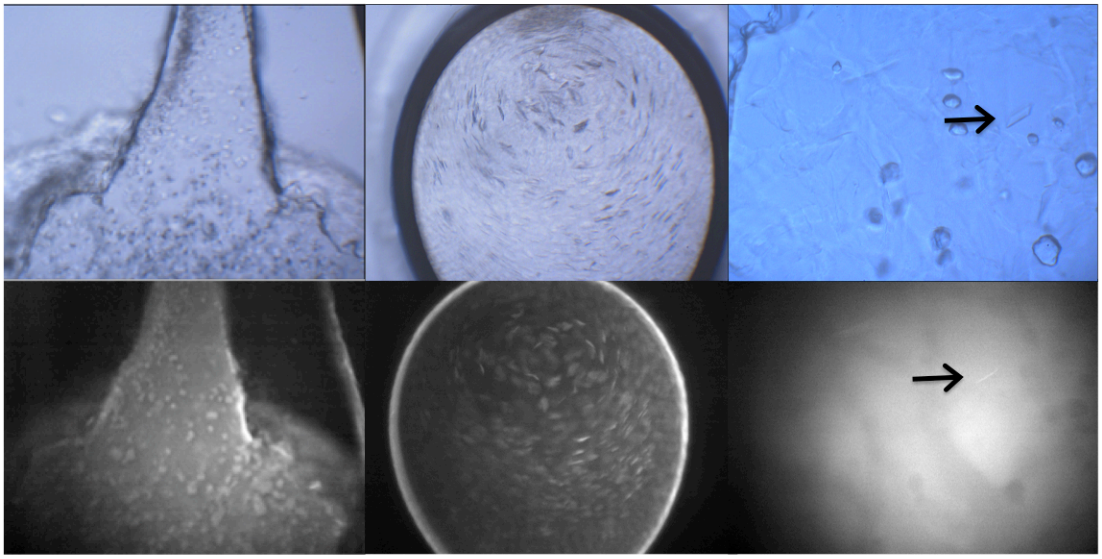

Figure S10: Visible light (top) and UV (bottom) images of M2 crystals. Square-shaped plates of M2TM bound to drugs and inhibitors form in the lipid cubic phase.

Table S1. Structural and dynamic measures from 250 ns MD trajectories of M2TM-ligand complexes in POPC bilayer at high pH.

Ligand	RMSD (Cα 27-46) [1]	RMSD Achain (Cα 27-46) [2]	RMSD Bchain (27-46) [3]	RMSD Cchain (27-46) [4]	RMSD Dchain (27-46) [5]
Amt	0.90 ± 0.2	0.76 ± 0.1	0.75 ± 0.1	0.64 ± 0.1	0.62 ± 0.1
Rim-*R*	0.97 ± 0.2	0.60 ± 0.1	0.53 ± 0.1	0.66 ± 0.1	1.03 ± 0.2
Rim-*S*	0.77 ± 0.2	0.61 ± 0.1	0.56 ± 0.1	0.64 ± 0.1	0.55 ± 0.1
Spiro-adamantyl amine	0.96 ± 0.2	0.60 ± 0.1	0.62 ± 0.1	0.58 ± 0.1	0.93 ± 0.2

Ligand	Ligand tilt	V27-Ad [8]	A30-Ad [9]	G34-Ad [10]	H-bonds [11]	Cl-N distance [12]
Amt	11.5 ± 6.1 [6]	4.5 ± 0.3	0.7 ± 0.3	5.2 ± 0.3	2.8 ± 0.4	51.0 ± 10.7
Rim-*R*	21.7 ± 7.7 [6]	4.2 ± 0.3	1.1 ± 0.3	5.7 ± 0.3	3.0 ± 1.1	47.2 ± 10.1
Rim-*S*	17.4 ± 5.7 [6]	4.3 ± 0.3	1.0 ± 0.3	5.5 ± 0.3	2.9 ± 1.1	47.1 ± 10.4
Spiro-adamantyl amine	8.2 ± 4.1 [7]	4.3 ± 0.3	1.0 ± 0.3	5.4 ± 0.3	2.7 ± 0.5	49.0 ± 10.6

[1] Root-mean-square deviation (RMSD) for Cα atoms of M2TM tetramer, residues 27-46, relative to the initial structure (PDB entry: 6BKK, 6BKL, 6BMZ respectively) after root-mean-square fitting of Cα atoms; in Å.

[2-5] Root-mean-square deviation (RMSD) for Cα atoms of M2TM helix A-D, residues 27-46, relative to the initial structure (PDB entry: 6BKK, 6BKL, 6BMZ respectively) after root-mean-square fitting of Cα atoms; in Å.

[6] Angle between the adamantane C3 symmetry axis vector and the normal to the membrane; in degrees.

[7] Angle between the adamantane C2 symmetry axis vector and the normal to the membrane; in degrees.

[8] Mean distance between center of mass of V27 and centers of mass of adamantane calculated using Gromacs tools; in Å.

[9] Mean distance between center of mass of A30 and centers of mass of adamantane calculated using Gromacs tools; in Å.

[10] Mean distance between center of mass of G34 and centers of mass of adamantane calculated using Gromacs tools; in Å.

[11] Mean number of H-bonds between ligand's ammonium group and waters.
[12] Mean distance in Å between the ligand N and the nearest Cl^-.

Structure	**6BKK**	**6BKL**	**6BMZ**	**6BOC**
Space group	$P2_1$	$P2_1$	$P2_12_12_1$	P2
Cell dimensions (Å)				
a,b,c (Å)	44.22, 52.05, 48.72	36.46, 47.84, 48.53	49.62, 72.59, 99.25	34.05, 34.02, 72.09
α, β, γ (°)	90.00, 108.2, 90.00	90.00, 96.76, 90.00	90.00, 90.00, 90.00	90.00, 90.23, 90.00
Resolution (Å)	52.05 - 2.00 (2.05 - 2.00)	48.19 - 2.00 (2.05 - 2.00)	72.59 - 2.63 (2.76 - 2.63)	36.04 - 2.25 (2.32 - 2.25)
Completeness (%)	93.5 (88.8)	93.3 (90.8)	99.3 (98.9)	98.3 (96.3)
Number of unique reflections	13454 (942)	10589 (754)	11007 (1442)	7894 (695)
Average redundancy	2.2 (2.1)	4.8 (4.5)	7.0 (6.9)	3.2 (3.3)
Rmerge	0.164 (0.808)	0.114 (0.348)	0.154 (0.608)	0.203 (0.463)
CC(1/2)	0.974 (0.508)	0.994 (0.959)	0.997 (0.920)	0.957 (0.791)
Average I/sigI	4.6 (2.2)	7.1 (2.9)	8.7 (3.0)	4.2 (2.1)

Table S2: Data processing statistics for M2 bound to amantadine (6BKK), rimantadine (6BKL), and spiro-adamantyl amine (6BMZ) in the $Inward_{closed}$ conformation, and M2 bound to rimantadine (6BOC) in the $Inward_{open}$ conformation. Data processing was carried out in Aimless,[3] with space group validation in Zanuda.[4]

Structure	6BKK	6BKL	6BMZ	6BOC
Resolution (Å)	46.29 - 1.995 (2.066 - 1.995)	48.19 - 1.995 (2.066 - 1.995)	44.38 - 2.634 (2.728 - 2.634)	34.05 - 2.25 (2.33 - 2.25)
Number of reflections refined against	13419 (1269)	10543 (1022)	10945 (1075)	7886 (747)
Completeness (working + test) (%)	92.83 (89.05)	92.24 (89.81)	98.49 (98.53)	97.74 (95.77)
Rwork	0.2271 (0.2443)	0.1863 (0.2019)	0.2255 (0.2608)	0.2600 (0.2785)
Rfree	0.2703 (0.3112)	0.2439 (0.2892)	0.2767 (0.3376)	0.2815 (0.4070)
Number of non-hydrogen atoms	1680	1538	3115	849
Macromolecules	1536	1452	2964	768
Ligands	39	52	84	44
Water	105	34	67	37
Ramachandran favored (%)	100	100	99.14	100
RMS(bonds)	0.001	0.007	0.002	0.015
RMS(angles)	0.33	0.75	0.44	1.23
Average B-factor	15.95	28.49	29.20	32.96
Macromolecules	14.99	28.41	28.83	31.85
Ligands	21.01	26.92	32.62	42.70
Water	28.14	34.42	41.39	44.62

Table S3: Refinement statistics for M2 bound to amantadine (6BKK), rimantadine (6BKL), and spiro-adamantyl amine (6BMZ) in the $Inward_{closed}$ conformation, and M2 bound to rimantadine in the $Inward_{open}$ conformation (6BOC). Refinement was carried out in PHENIX.refine[5] with model-building in Coot[6] and PyMOL.[7]

Experimental methods:

The construct of M2 used in this study was Influenza A/Udorn/1972 M2 wild-type, residues 22-46. The peptide was chemically synthesized and purified as previously described,[8, 9] with acetylation of the N-terminus and amidation of the C-terminus: Ace-SSDPLVVAASIIGILHLILWILDRL-NH2

The peptide sample was reconstituted into the lipid cubic phase (LCP) with some modifications to Caffrey and Cherezov's protocol.[10] Dry peptide was dissolved in ethanol and added directly to monoolein powder. Excess ethanol was blown off with nitrogen gas, and the sample was left under vacuum (<100 mTorr) overnight to remove the remaining solvent.

The drugs and inhibiting compounds used in this study were amantadine (1-adamantylamine HCl, Aldrich), rimantadine (1-(1-adamantyl)ethylamine HCl, Aldrich), and spiro-adamantyl amine "Compound 9" from Wang et al. 2011.[11] These compounds were added as ethanol stock solutions to the peptide plus monoolein mixture described above, before removal of excess solvent.

The lipid cubic phase was made by mixing 30 mg of peptide/monoolein sample with 20 μL of 50 mM detergent solution using two syringes connected by a syringe coupler at a temperature of 40 ˚C. The detergent used in this study was a maltose neopentyl glycol analogue, MNG-3-C8 ($C_{43}H_{80}O_{22}$, MW = 949.08). MNG detergents have been observed to stabilize membrane proteins for crystallization trials.[12,13] The MNG-3-C8 detergent was synthesized by the Pil Seok Chae group (Hanyang University, Seoul, South Korea). Plastic 96-well LCP sandwich trays (Laminex, 200 micron base) containing drops of LCP plus precipitant solution were used to screen crystallization conditions using a LCP crystallization robot (TTP Labtech). Trays were screened using visible-light and UV imaging. Crystals were harvested from 96-well trays and frozen in liquid nitrogen for transport and data collection.

The crystals formed by these conditions were thin, square-shaped plates. Though a detergent amphiphile was present in the crystallization conditions, the protein-containing lipid cubic phase remained separate from the precipitant solution and did not swell into the sponge phase. The crystallization conditions yielding the deposited PDB structures are as follows:

6BKK: 100 nL LCP + 1 μL precipitant solution. LCP: 60 mg monoolein, 1.6 x 10^{-6} moles M2TM (EtOH stock), 6.4 x 10^{-6} amantadine (EtOH stock) (4:1 ratio of amantadine:M2 monomer); 40 μL of 50 mM MNG-3-C8 detergent in water. Precipitant solution: 0.1 M NaCl, 0.02 M sodium citrate pH 5.6, 11% w/v PEG 3350. Crystals grew at 20 ˚C. Thin square plates formed after 9 months and grew to 100 μm in size.

6BKL: 100 nL LCP + 0.5 μL precipitant solution. LCP: 60 mg monoolein, 1.6 x 10^{-6} moles M2TM (EtOH stock), 6.4 x 10^{-6} moles rimantadine (EtOH stock) (4:1 ratio of rimantadine:M2 monomer); 40 μL of 50 mM MNG-3-C8 detergent in water. Precipitant solution: 0.2 M $MgCl_2$, 0.1 M sodium acetate / acetic acid pH 4.5, 20% w/v PEG 8000. Plates were incubated at 20 ˚C. Thin square plates formed after 1 month and grew to 75 μm in size.

6BMZ: 100 nL LCP + 0.5 μL precipitant solution. LCP: 60 mg monoolein, 1.6 x 10^{-6} moles M2TM (EtOH stock), 6.4 x 10^{-6} moles spiro-adamantyl amine (EtOH

stock) (4:1 ratio of inhibitor:M2 monomer); 40 µL of 50 mM MNG-3-C8 detergent in water. Precipitant solution: 0.1 M HEPES pH 7.0, 30% v/v PEG 400. Plates were incubated at 20 ˚C. Thin square plates formed after 1 week and grew to 50 µm in size.

6BOC: 100 nL LCP + 0.5 µL precipitant solution. LCP: 2.4 x 10^{-6} moles M2TM (EtOH stock), 9.6 x 10^{-6} moles rimantadine (EtOH stock) (4:1 ratio of rimantadine:M2 monomer); 40 µL of 50 mM MNG-3-C8 detergent in water. Precipitant solution: 0.18 M LiSO4, 4% v/v (±)-1,3-butanediol, 0.09 M sodium citrate pH 3.5 (adjusted w/ HCl), 25.2% v/v PEG 400. Thin square plates formed after 2 weeks and grew to 300 µm in size.

Data were collected at Advanced Light Source (ALS) beam 8.3.1. 6BKK, 6BKL, and 6BMZ were collected using a Q315 detector. 6BOC was collected using a Pilatus 6M detector. Data collection parameters were as follows:
6BKK: E = 11111 eV, d = 250 mm, oscillation = 1˚, t = 2 s, 115 frames.
6BKL: E = 11111 eV, d = 250 mm, oscillation = 1˚, t = 1 s, 360 frames.
6BMZ: E = 11111 eV, d = 350 mm, oscillation = 1˚, t = 1 s, 200 frames.
6BOC: E = 11111 eV, d= 300 mm, oscillation = 0.7˚, t = 0.2 s, 300 frames.

Indexing and integration were carried out in MOSFLM,[14] and the data were scaled and merged using Aimless[3] in the CCP4 suite.[15, 16] Molecular replacement was done using Phaser[17] with previously solved structures as search models (3LBW[18] for the $Inward_{closed}$ state, 4QK7[8] for the $Inward_{open}$ state). Zanuda[4] was used to aid in space group determination. Refinement was carried out in PHENIX,[5] with model building in Coot[6] and PyMOL.[7]

The tilts of amantadine and rimantadine adamantyl groups relative to the channel's central axis for structures 6BKK and 6BKL were calculated as the angle between two vectors: the channel central axis vector, and the adamantyl 3-fold axis vector. The channel central axis vector consists of the averaged Cα coordinates for all four monomers of the tetramer at two different residues, Leu26 and His37. The adamantyl 3-fold axis vector consists of the averaged coordinates of three symmetrically equivalent adamantyl carbons (atom names C2, C4, and C6 for amantadine, and atom names CG1, CG2, and CG3 for rimantadine), and the coordinates of an atom at the center of the 3-fold axis (atom name C10 for amantadine, and atom name CD for rimantadine).

Molecular dynamics methods:
The M2TM were embedded in a POPC lipid bilayer extending 30 Å beyond the solutes. The number of lipids added was ~ 200. The bilayer was then solvated by a 30-Å-thick layer of waters. Na^+ and Cl^- ions were placed in the water phase to neutralize the systems and to reach the experimental salt concentration of 0.150 M NaCl. The total number of ions was ~ 80000. Membrane creation and system solvation were conducted with the "System Builder" utility of Desmond. The OPLS 2005 force field[19-21] was used to model all protein and ligand interactions, and the TIP3P[22] model was used for water. The particle mesh Ewald method (PME)[23, 24] was employed to calculate long-range electrostatic interactions with a grid spacing of 0.8

Å. Van der Waals and short range electrostatic interactions were smoothly truncated at 9.0 Å. The Nosé-Hoover thermostat[25] was utilized to maintain a constant temperature in all simulations, and the Martyna-Tobias-Klein method[25] was used to control the pressure. Periodic boundary conditions were applied (90×90×105)Å^3. The equations of motion were integrated using the multistep RESPA integrator with an inner time step of 2 fs for bonded interactions and non-bonded interactions within a cutoff of 9 Å. An outer time step of 6.0 fs was used for non-bonded interactions beyond the cut-off. Each system was equilibrated in MD simulations with a modification of the default protocol provided in Desmond, which consists of a series of restrained minimizations and MD simulations designed to relax the system, while not deviating substantially from the initial coordinates. First, two rounds of steepest descent minimization were performed with a maximum of 2000 steps with harmonic restraints of 50 kcal mol^{-1} Å^{-2} applied on all solute atoms, followed by 10000 steps of minimization without restraints. The first simulation was run for 200 ps at a temperature of 10 K in the NVT ensemble with solute heavy atoms restrained with a force constant of 50 kcal mol^{-1} Å^{-2}. The temperature was then raised during a 200 ps MD simulation to 310 K in the NVT ensemble with the force constant retained. The heating was followed by equilibration runs. First, two stages of NPT equilibration were performed, one with the heavy atoms of the system restrained for 1 ns and one for solvent and lipids for 10 ns, with a force constant of 10 kcal/mol/Å^2 for the harmonic constraints, respectively. A NPT simulation followed with the C_α atoms restrained for 1ns with a force constant of 2 kcal/mol/Å^2. The above-mentioned equilibration was followed by a 250ns NPT simulation without restraints. Within this time, the total energy and the RMSD reached a plateau, and the systems were considered equilibrated. For structural analyses, snapshots of the different systems were created with VMD[26] or Maestro[27] or Chimera[28]. Trajectories were analyzed with Maestro, Gromacs,[29, 30] and VMD. Measurements were carried out with Gromacs tools. For the calculation of hydrogen bonds, a cut-off angle of 30^o deviation from 180^o between the donor-hydrogen-acceptor atoms and a cut-off distance of 3.5 Å between the donor and acceptor atoms were applied.

Molecular Dynamics Analysis

We analyzed snapshots at 5 ps intervals of the 100 ns trajectory. Snapshots were aligned to the M2 crystal structure via CA atoms of residues 26-42.

Autocorrelation

Autocorrelation functions of **Figs. S5** and **S7** were calculated by:

$$C(t) = (\langle A(0)A(t) \rangle - \langle A \rangle^2) / (\langle A^2 \rangle - \langle A \rangle^2)$$

where A is the variable of interest, and were fit to a mono- or bi-exponential decay function. For angular data, we fit the autocorrelation of the cosine of the angle.

Intrinsic Spin

Intrinsic spin was calculated by the following procedure: An internal reference frame of the drug was rotated about the X and Y axes of the bundle. The

intrinsic spin is the final rotation about the Z axis (long axis of the bundle) to align the drug internal reference frame with the reference frame of the bundle. For intrinsic spin of the amine, the internal reference frame was taken as the following (normalized) vectors:

Amine of amantadine:

origin = center of mass of amine hydrogens
z-axis = C1 – origin
x-axis = H1A – origin
y-axis = z ⊗ x

Amine of spiro-adamantyl amine:

origin = center of mass of amine hydrogens
z-axis = C10 – origin
x-axis = HN1 – origin
y-axis = z ⊗ x

Adamantane of amantadine:

origin = center of mass of C7, C8, C9
z-axis = N1 – origin
x-axis = C8 – origin
y-axis = z ⊗ x

Adamantane of Spiro-adamantyl amine:

origin = center of mass of C8, C10, C14, C15
z-axis = C4 – origin
x-axis = C8 – origin
y-axis = z ⊗ x

Clustering of MD snapshots by amine position

After superposition of the snapshots onto the crystal structure as described above, we used a greedy clustering method (see Daura et al.[31]) to cluster the MD snapshots by position of the amine, including hydrogens. No further manipulation of the amine coordinates was taken. Atoms used in the RMSD calculation were C10, N1, HN1, HN1A, and HN1B for amantadine and C1, N1, H1A, H1B, and HIC for spiro-adamantyl amine. The amines were clustered with a 0.6 Å RMSD. At this cutoff, greater than 50% of the MD snapshots were placed into the top 2 (amantadine) or 3 (spiro-adamantyl amine) clusters. All permutations of the hydrogens were considered in the clustering. The positions of the waters from these top clusters are shown in the water density figures.

(1) Liebschner, D.; Afonine, P. V.; Moriarty, N. W.; Poon, B. K.; Sobolev, O. V.; Terwilliger, T. C.; Adams, P. D. *Acta Crystallogr. D* **2017,** *73* (Pt 2), 148-157.

(2) Stouffer, A. L.; Acharya, R.; Salom, D.; Levine, A. S.; Di Costanzo, L.; Soto, C. S.; Tereshko, V.; Nanda, V.; Stayrook, S.; DeGrado, W. F. *Nature* **2008,** *451* (7178), 596-U13.
(3) Evans, P. *Acta Crystallogr. D* **2006,** *62* (1), 72-82.
(4) Lebedev, A. A.; Isupov, M. N. *Acta Crystallogr. D* **2014,** *70* (9), 2430-2443.
(5) Adams, P. D.; Afonine, P. V.; Bunkoczi, G.; Chen, V. B.; Davis, I. W.; Echols, N.; Headd, J. J.; Hung, L. W.; Kapral, G. J.; Grosse-Kunstleve, R. W.; McCoy, A. J.; Moriarty, N. W.; Oeffner, R.; Read, R. J.; Richardson, D. C.; Richardson, J. S.; Terwilliger, T. C.; Zwart, P. H. *Acta Crystallogr. D* **2010,** *66*, 213-221.
(6) Emsley, P.; Lohkamp, B.; Scott, W. G.; Cowtan, K. *Acta Crystallogr. D* **2010,** *66*, 486-501.
(7) Schrodinger, LLC, The PyMOL Molecular Graphics System, Version 1.3r1. 2010.
(8) Thomaston, J. L.; Alfonso-Prieto, M.; Woldeyes, R. A.; Fraser, J. S.; Klein, M. L.; Fiorin, G.; DeGrado, W. F. *J. Proc. Natl. Acad. Sci. U. S. A.* **2015,** *112* (46), 14260-14265.
(9) Thomaston, J. L.; DeGrado, W. F. *Protein Sci.* **2016,** *25* (8), 1551-1554.
(10) Caffrey, M.; Cherezov, V. *Nat. Protoc.* **2009,** *4* (5), 706-731.
(11) Wang, J.; Ma, C. L.; Fiorin, G.; Carnevale, V.; Wang, T.; Hu, F. H.; Lamb, R. A.; Pinto, L. H.; Hong, M.; Kein, M. L.; DeGrado, W. F. *J. Am. Chem. Soc.* **2011,** *133* (32), 12834-12841.
(12) Chae, P. S.; Rasmussen, S. G. F.; Rana, R.; Gotfryd, K.; Chandra, R.; Goren, M. A.; Kruse, A. C.; Nurva, S.; Loland, C. J.; Pierre, Y.; Drew, D.; Popot, J.-L.; Picot, D.; Fox, B. G.; Guan, L.; Gether, U.; Byrne, B.; Kobilka, B.; Gellman, S. H. *Nat. Methods* **2010,** *7* (12), 1003-1008.
(13) Cho, K. H.; Husri, M.; Amin, A.; Gotfryd, K.; Lee, H. J.; Go, J.; Kim, J. W.; Loland, C. J.; Guan, L.; Byrne, B.; Chae, P. S. *Analyst* **2015,** *140* (9), 3157-3163.
(14) Battye, T. G. G.; Kontogiannis, L.; Johnson, O.; Powell, H. R.; Leslie, A. G. W. *Acta Crystallogr. D* **2011,** *67*, 271-281.
(15) Cowtan, K.; Emsley, P.; Wilson, K. S. *Acta Crystallogr. D* **2011,** *67* (4), 233-234.
(16) Winn, M. D.; Ballard, C. C.; Cowtan, K. D.; Dodson, E. J.; Emsley, P.; Evans, P. R.; Keegan, R. M.; Krissinel, E. B.; Leslie, A. G. W.; McCoy, A.; McNicholas, S. J.; Murshudov, G. N.; Pannu, N. S.; Potterton, E. A.; Powell, H. R.; Read, R. J.; Vagin, A.; Wilson, K. S. *Acta Crystallogr. D* **2011,** *67* (Pt 4), 235-242.
(17) McCoy, A. J.; Grosse-Kunstleve, R. W.; Adams, P. D.; Winn, M. D.; Storoni, L. C.; Read, R. J. *J. Appl. Crystallogr.* **2007,** *40*, 658-674.
(18) Acharya, R.; Carnevale, V.; Fiorin, G.; Levine, B. G.; Polishchuk, A. L.; Balannik, V.; Samish, I.; Lamb, R. A.; Pinto, L. H.; DeGrado, W. F.; Klein, M. L. *Proc. Natl. Acad. Sci. U. S. A.* **2010,** *107* (34), 15075-80.
(19) Jorgensen, W. L.; Maxwell, D. S.; Tirado-Rives, J. *J. Am. Chem. Soc.* **1996,** *118* (45), 11225-11236.
(20) Kaminski, G. A.; Friesner, R. A.; Tirado-Rives, J.; Jorgensen, W. L. *J. Phys. Chem. B* **2001,** *105* (28), 6474-6487.
(21) Rizzo, R. C.; Jorgensen, W. L. *J. Am. Chem. Soc.* **1999,** *121* (20), 4827-4836.

(22) Jorgensen, W. L.; Chandrasekhar, J.; Madura, J. D.; Impey, R. W.; Klein, M. L. *J. Chem. Phys.* **1983,** *79* (2), 926-935.
(23) Darden, T.; York, D.; Pedersen, L. *J. Chem. Phys.* **1993,** *98* (12), 10089-10092.
(24) Essmann, U.; Perera, L.; Berkowitz, M. L.; Darden, T.; Lee, H.; Pedersen, L. G. *J. Chem. Phys.* **1995,** *103* (19), 8577-8593.
(25) Martyna, G. J.; Tobias, D. J.; Klein, M. L. *J. Chem. Phys.* **1994,** *101* (5), 4177-4189.
(26) Humphrey, W.; Dalke, A.; Schulten, K. *J. Mol. Graph.* **1996,** *14* (1), 33-38.
(27) Schrodinger, L. **2008**.
(28) Pettersen, E. F.; Goddard, T. D.; Huang, C. C.; Couch, G. S.; Greenblatt, D. M.; Meng, E. C.; Ferrin, T. E. *J. Comput. Chem.* **2004,** *25* (13), 1605-1612.
(29) Berendsen, H. J. C.; van der Spoel, D.; van Drunen, R. *Comput. Phys. Commun.* **1995,** *91* (1), 43-56.
(30) Hess, B.; Kutzner, C.; van der Spoel, D.; Lindahl, E. *J. Chem. Theory Comput.* **2008,** *4* (3), 435-447.
(31) Xavier, D.; Karl, G.; Bernhard, J.; Dieter, S.; F., v. G. W.; E., M. A. *Angew. Chem.* **1999,** *38* (1 ‐ 2), 236-240.